JOURNAL OF CATALYSIS 126, 279–290 (1990)

Carbon Gasification by Group VIII Metal Catalysts

MARK E. VINCETT, JOHN A. TSAMOPOULOS, AND CARL R. F. LUND

Chemical Engineering Department, State University of New York, Buffalo, New York 14260

Received April 2, 1990; revised June 8, 1990

A mathematical model for the steam gasification of carbon using group VIII transition metal catalysts has been developed. The reaction mechanism is assumed to involve the dissolution of carbon into the metal catalyst at the front half of the spherical particle followed by diffusion of carbon through the particle and finally reaction on the surface of the rear half of the particle. A material balance on the carbon within the catalyst is then written both for the steady-state and unsteady reaction. The steady-state model reproduces the experimentally observed dependence of the rate of reaction upon particle size as well as a change in the apparent activation energy of the reaction. The model suggests that the change in apparent activation energy occurs as the rate-determining step changes from diffusion of carbon through the particle (at low temperature) to surface reaction rate. The unsteady model can qualitatively and quantitatively show the experimentally observed deactivation of the catalyst, but it does not have complete predictive capability because there are too many unknown physical constants.

INTRODUCTION

Group VIII metals, and especially nickel, are very active as catalysts in the steam gasification of carbon (*1–6*). In fact, they are much more active than potassium or calcium, especially at low temperatures which would be desirable for methane production (*7, 8*). Still, if catalytic gasification of coal was to be implemented commercially at present, an alkali or alkaline-earth catalyst would probably be used. The group VIII ferrous metals show some promise when used in conjunction with an alkaline-earth material like calcium (*9, 10*), but when used alone, they tend to deactivate (*1–3, 6–9, 11, 12*). Deactivation can be caused by interaction with mineral matter in the coal, by poisoning of the catalyst by heteroatoms like halides or sulfur, or just as a consequence of the reaction, as discussed below.

By considering "pure" carbons instead of coal or coal char, the first two causes of deactivation are eliminated. The deactivation, e.g., of nickel, during steam or CO_2 gasification of pure carbons and graphite has been observed many times (*1–3, 6–9, 11, 12*). In some instances deactivation occurs because the group VIII metal catalyst becomes oxidized (*1, 9, 10*), but even under reaction conditions where the metal remains reduced, the catalyst can deactivate (*11, 12*). In this situation (pure carbon, fully reduced catalyst) deactivation is a result of (i) a reduction in the interfacial contact area between the catalyst and the carbon, (ii) a reduction in the interfacial contact area between the catalyst and the gas phase, or (iii) a decrease in both interfacial contact areas (i.e., catalyst sintering) (*12*).

Many studies have shown that the catalysts do indeed sinter, but the amount of sintering is not sufficient to explain the deactivation observed. In one investigation (*12*), *both* the total surface area and the interfacial contact area between the catalyst and the gas phase were measured as the catalyst underwent deactivation. This revealed that graphite and an active carbon suffer catalyst deactivation for different reasons.

During the gasification of graphite, the interfacial contact area between the catalyst and the graphite preferentially decreases as the catalyst deactivates (*12*). This has been explained by the "piling up" of catalyst particles on the graphite surface such that many

0021-9517/90 $3.00

of the catalyst particles contact only the gas phase and other catalyst particles. Since the "piled up" catalysts do not contact the graphite, they cannot activate carbon atoms, and hence they are inactive. At the beginning of the reaction, especially for low loadings of catalyst, each particle is active and catalyzes gasification at a steady-state rate. The present paper begins with the development of a steady-state model of a single catalyst particle under such circumstances.

Previous models for the catalytic gasification of carbon by group VIII metals have all sought to explain the dependence of the rate of channeling upon the catalyst particle diameter which has been observed directly via controlled atmosphere electron microscopy. Generally the rate is inversely proportional to the square root of the particle diameter (see Fig. 2). The first successful model of this behavior (*13*) used a cubic particle, it allowed only one exposed surface of the cube to catalyze gasification, and it used diffusivities, solubilities, and other parameters from different metals in a single model. Still, it was successful in reproducing the observed behavior.

A later model of the hydrogen gasification of carbon (*14*) was used to show that the rate-limiting step in the case of hydrogen gasification using Ru catalyst was not the diffusion of the carbon through the metal, but the surface reaction step. The computed flux of carbon through the particle by diffusion was an order of magnitude greater than the flux observed during reaction, i.e., the reaction rate.

Later still, a model was developed which was capable of explaining rate versus diameter data for both the hydrogen gasification reaction and the gasification in oxidizing atmospheres (*15*). In this model the particle was taken as a cylinder, and it was recognized that the particle did not deform, and consequently the front face could not be saturated at all locations because this would lead to different rates of dissolution of carbon across the face of the catalyst.

The present model is also capable of predicting the dependence of the rate of channeling upon the particle diameter. It uses a more realistic particle shape than the previous models. More importantly, the model can also be used to calculate the dependence of reaction rate upon temperature. When plotted in Arrhenius fashion, experimental data indicate a change in activation energy, and this model predicts such a change. Furthermore, it provides a physical interpretation for this change in activation energy which differs from the previously assumed cause (onset of mass transfer limitations).

When active carbon is being gasified the interfacial contact area between the catalyst and the gas phase preferentially decreases as the catalyst deactivates (*12*). This has been explained by the formation of a graphitic carbon overlayer on the surface of the metal, effectively blocking the gas phase from making contact with the metal. A thermodynamic driving force exists for the formation of graphite from activated carbons. The present paper also extends the steady-state model alluded to previously to include the unsteady growth of a graphitic overlayer leading to catalyst deactivation.

FORMULATION OF THE MODELS

1. Steady-State Model

The mechanism of gasification of carbon by group VIII metal catalysts is generally accepted to begin with the dissolution of carbon from the substrate into the metal at a surface which is in contact with the carbon. This is followed by the diffusion of carbon through or over the metal particle to a surface which is in contact with the gas phase (*13–16*). The carbon on this surface (in contact with the gas phase) would be expected to initially be carbidic (*17*) in nature. At the same time, the gas phase H_2O/H_2 or CO_2/CO ratio establishes a steady-state coverage of this surface with adsorbed oxygen. The carbidic carbon and the adsorbed oxygen finally react to produce CO completing the gasification mechanism. This mechanism requires that the catalyst move into the carbon

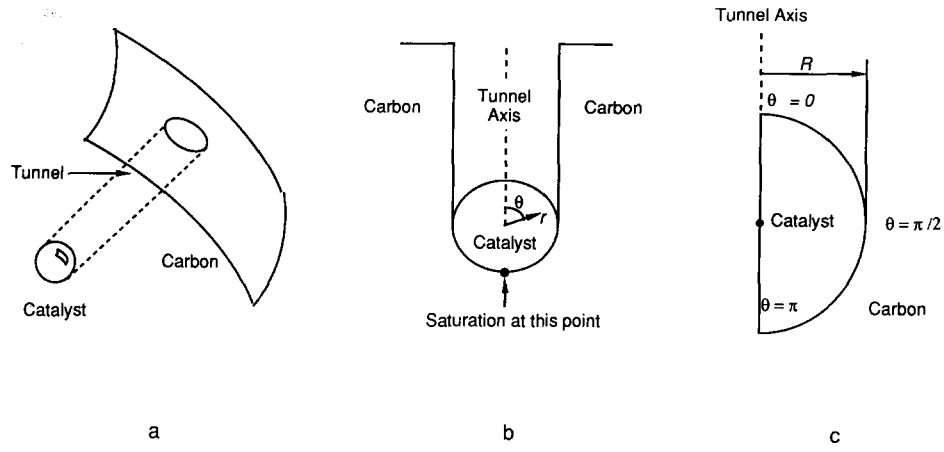

FIG. 1. (a) A schematic representation of the gasification process, (b) a cross section through a catalyst particle along the tunnel axis, and (c) the coordinate system used in the model.

in order to maintain contact with the carbon as it is gasified. This has been observed directly for the gasification of graphite (*5, 16*), where the anisotropy of the carbon results in two-dimensional motion of the catalyst on the graphite surface. The phenomenon has been called channeling. When an active carbon is gasified, the reactivity is expected to be isotropic; catalyst motion in this case will be referred to as tunneling. Previous models of catalytic gasification (*13–15*) have all included these basic features.

In the present model the particle is assumed to be spherical, of radius R, with one hemisphere (henceforth called the front) in contact with the substrate which is active carbon and the other hemisphere in contact with the gas phase. This is represented schematically in Fig. 1. The z direction is taken to lie along the axis of the tunnel with the origin at the center of the particle. The particle is symmetrical with respect to the angle about the z axis, and consequently the model is developed in two spatial dimensions, r and θ, the angle measured from the z axis. The front of the catalyst (contacting the carbon) corresponds to $0.5\pi \leq \theta < \pi$; the rear of the catalyst corresponds to $0 \leq \theta < 0.5\pi$. A steady-state mass balance on carbon within a differential volume element inside the catalyst particle results in

$$\mathcal{D}\nabla^2 C = 0. \qquad (1)$$

In Eq. (1) $\mathcal{D}$ is the diffusion coefficient of carbon in the metal and is only a function of temperature, ∇^2 is the Laplacian operator in spherical coordinates, and C is the concentration of carbon. Equation (1) further assumes that there is no convection within the catalyst. The reaction temperature is well below the bulk melting point of the catalyst. Hence, assuming that ordinary solid-state diffusion is the only mode of carbon transport is justified. It is further assumed that the catalyst particle is isothermal. This assumption has been justified by calculation (*18, 19*), although it has been suggested elsewhere that a substantial temperature gradient might exist within small particles (*20*).

Earlier models assumed that the front surface of the catalyst was everywhere saturated with dissolved carbon. Recently it was pointed out (*15*) that the particle does not deform if it moves at constant speed as has been experimentally observed. Actually, the particles do deform as they first make contact with the edges of the graphite planes. However, for the ferrous metals in steam and CO_2, the particles maintain a nearly constant shape once they have attained a steady-state rate of channeling. (Other Group VIII metals, especially during

oxygen gasification, are much more liquid-like under reaction conditions. The steady-state particle shape which is attained is not perfectly spherical either, but it is close to spherical. The assumption of a spherical shape is not expected to have a significant effect upon the conclusions resulting from the model.) When the shape of the particle is constant, it is more appropriate to require that the flux of carbon through a plane perpendicular to the direction of motion of the catalyst particle must be uniform than to assume saturation across the entire front surface. This means that only the point on the front surface which presents the longest diffusion path to the carbon can be at the saturation concentration, C^*. In the present geometry this point lies on the tunnel axis at the front surface. On the remainder of the front surface the flux of carbon in the direction of motion of the catalyst particle will equal the flux at this point. This forms the boundary condition for the front hemisphere.

$$C = C^* \quad \text{at } r = R,\ \theta = \pi \tag{2a}$$

$$\frac{1}{\cos\theta}\frac{\partial C}{\partial r} = K \quad \text{at } r = R,\ \pi/2 \le \theta \le \pi. \tag{2b}$$

The constant K in Eq. (2b) is calculated so that Eq. (2a) holds.

The fractional coverage of the rear surface by carbidic carbon, Θ_C, is assumed to equal the atomic fraction of carbon dissolved in the metal just below the surface (i.e., $\Theta_C = C/(C + \rho/M) \approx MC/\rho$, where M is the molecular weight and ρ is the density of Ni). A constant fraction, f, of the remainder of the surface, $(1 - \Theta_C)$, is assumed to be covered by oxygen in pseudo-equilibrium with the gas phase mixture of H_2/H_2O. A uniform surface model is used to generate the rate expression, Eq. (3), for the disappearance of carbidic carbon by reaction with surface oxygen:

$$q = k_1\Theta_C(1 - \Theta_C)S^2 = k_1'\Theta_C(1 - \Theta_C). \tag{3}$$

In Eq. (3) q is the rate of the surface reaction in moles of carbon per unit surface area per unit time, S is the molar site density (moles of surface sites per unit surface area), and k_1 is the rate constant for the reaction; the latter quantity also includes the fraction of the non-carbide-covered surface which is covered by oxygen, f. The site density was equal to the surface density of Ni atoms in the (100) surface. At steady state the rate of the surface reaction must just equal the rate at which carbidic carbon reaches the surface by diffusion, $-\mathcal{D}(\partial C/\partial r)|_{r=R}$. This forms the boundary condition for the rear hemisphere.

2. Unsteady Model

A mass balance on carbon within a differential volume element inside the catalyst particle results in Eq. (4) when the system is not at steady state:

$$\frac{\partial C}{\partial t} = \mathcal{D}\nabla^2 C. \tag{4}$$

In Eq. (4) t represents the time. The boundary conditions at the front surface of the catalyst are not changed from the steady-state boundary conditions.

At the rear surface of the catalyst there are two surface reactions allowed in the unsteady model. The first is the reaction of carbidic carbon to yield gasification products. The only change in the rate expression for this reaction arises from the fact that as the graphitic overlayer forms, the fraction of the surface which it occupies, Θ_G, is no longer available for the adsorption of oxygen. Thus, the rate expression is given by

$$q = k_1\Theta_C(1 - \Theta_C - \Theta_G)S^2 = k_1'\Theta_C(1 - \Theta_C - \Theta_G). \tag{5}$$

There is a second reaction at the rear surface in the unsteady model, namely the growth of the graphitic overlayer. This reaction is taken to involve the reaction between two surface carbidic carbons to form surface graphitic carbon. This is a simplistic picture, and uniform surface kinetics yield Eq. (6) as the rate expression for the reaction:

TABLE 1

A Summary of the Two Models

	Steady-state model	Unsteady model
Material balance	$\mathcal{D}\nabla^2 C = 0$	$\frac{\partial C}{\partial t} = \mathcal{D}\nabla^2 C$
Boundary condition at the front surface ($r = R$ and $0.5\pi \leq \theta < \pi$)	$C = C^*$ at $r = R$; $\theta = \pi$ $\frac{1}{\cos\theta}\frac{\partial C}{\partial r} = K$ at $r = R$, $\pi/2 \leq \theta \leq \pi$	$C = C^*$ at $r = R$; $\theta = \pi$ $\frac{1}{\cos\theta}\frac{\partial C}{\partial r} = K$ at $r = R$, $\pi/2 \leq \theta \leq \pi$
Boundary condition at the rear surface ($r = R$ and $0 \leq \theta < 0.5\pi$)	$-\mathcal{D}\frac{\partial C}{\partial r} = k_1\Theta_C(1 - \Theta_C)S^2$	$-\mathcal{D}\frac{\partial C}{\partial r} = k_1\Theta_C(1 - \Theta_C - \Theta_G)S^2 + k_2(\Theta_C)^2 S + S\frac{\partial \Theta_C}{\partial t}$
Symmetry condition for all r at $\theta = 0$ and $\theta = \pi$	$\frac{\partial C}{\partial \theta} = 0$	$\frac{\partial C}{\partial \theta} = 0$
Initial condition ($t = 0$)	Not applicable	$C = 0$ for all r and θ

$$\frac{\partial \Theta_G}{\partial t} = k_2(\Theta_C)^2 S = k_2'(\Theta_C)^2. \qquad (6)$$

In Eq. (6) k_2 is the surface normalized rate constant for the reaction which produces the graphitic overlayer. In the unsteady model, the rate at which carbidic carbon arrives at the rear surface via diffusion through the particle, $-\mathcal{D}(\partial C/\partial r)|_{r=R}$, is set equal to the sum of the rate at which it accumulates, $S(\partial\Theta_C/\partial t)$, and the rate at which it is consumed via the two surface reactions.

The unsteady model assumes that the particle is initially free of carbon everywhere. Due to the symmetry of the problem, it is only necessary to consider the region $0 \leq \theta < \pi$, and not any variations in the third direction. In doing so, the carbon concentration gradient in the θ direction is set equal to 0 at $\theta = 0$ and at $\theta = \pi$ for all r. This was done for both the steady-state and the unsteady models. Table 1 summarizes the equations and boundary conditions for each model.

The solubility and diffusivity of carbon in nickel are well studied, and experimental data for these properties as a function of temperature are readily available (*21–23*). Table 2 summarizes the values used in the model.

METHOD OF SOLUTION

The mass balance, Eq. (1) or (4), was solved using the finite element method. The computational domain is restricted to the hemisphere $0 \leq r \leq R$, $0 \leq \theta \leq \pi$, and it is discretized into a finite element mesh using isoparametric bilinear element basis functions $\{\phi_j\}$. This representation is written (*24*) as

$$C(r, \theta) = \sum_{j=1}^{N_1} \alpha_j \phi_i(r, \theta), \qquad (7)$$

where N_1 is the total number of unknown

TABLE 2

Physical Constants Used in the Models

Density of nickel, ρ	8.9117 g cm^{-3}
Concentration of carbon dissolved in Ni at saturation, C^*	8.87×10^{-2} exp{4880 K/T} mol cm^{-3}
Diffusion coefficient of carbon in Ni, $\mathcal{D}$	exp{0.909 − 20200 K/T} cm^2 s^{-1}

coefficients, $\{\alpha_j\}$, the values of which coincide with the carbon concentration at the nodes of the elements. A 20 × 20 uniform mesh was found sufficient to achieve solutions accurate to the fourth significant digit. Galerkin's principle is invoked, reducing Eq. (1) to a set of algebraic equations for the unknown constants $\{\alpha_j\}$. This requires that residuals obtained after substitution of Eq. (7) into Eq. (1) are orthogonal to the set of basis functions used, $\{\phi_j\}$. Then the weak form of the residual equations at every node is

$$R_j = -\mathcal{D}\int_0^{\pi}\int_0^{R} \nabla\phi_j \nabla C r^2 \sin\theta \, d\theta \, dr + R^2 K \mathcal{D}\int_{\pi/2}^{\pi} \phi_j \cos\theta \sin\theta \, d\theta - R^2 k_1' \int_0^{\pi/2} \Theta_C(1-\Theta_C)\phi_j \sin\theta \, d\theta = 0. \tag{8}$$

The K in Eq. (8) is the flux through the front of the particle (see Eq. (2b). Integration by parts has been used in order to reduce continuity requirements on the basis functions. As a result the flux and symmetry boundary conditions have been naturally incorporated in the equation set. The integrals are evaluated numerically by Gaussian quadrature (nine point for two-dimensional and three point for one-dimensional integrals). The algebraic set of equations (8) is solved by Gaussian elimination of the Jacobian matrix, J, the elements of which are derived by $J_{ji} = \partial R_j / \partial \alpha_i$.

For the solution of the unsteady-state problem, the unknown coefficients become functions of time, and using the same procedure, Eq. (4) reduces to an initial value problem for $\alpha_j(t)$:

$$\int_0^{\pi}\int_0^{R} \phi_j \frac{\partial C}{\partial t} r^2 \sin\theta \, d\theta \, dr = -\mathcal{D}\int_0^{\pi}\int_0^{R} \nabla\phi_j \nabla C r^2 \sin\theta \, d\theta \, dr + R^2 K \mathcal{D}\int_{\pi/2}^{\pi} \phi_j \cos\theta \sin\theta \, d\theta - R^2 k_1' \int_0^{\pi/2} \Theta_C(1-\Theta_C-\Theta_G)\phi_j \sin\theta \, d\theta - R^2 k_2' \int_0^{\pi/2} \Theta_C^2 \phi_j \sin\theta \, d\theta - R^2 S \int_0^{\pi/2} \phi_j \frac{\partial \Theta_C}{\partial t} \sin\theta \, d\theta, \tag{9}$$

where the last integral accounts for the production of graphitic carbon. Equation (6) must now be solved simultaneously with Eq. (9) by assuming

$$\Theta_G = \sum_{i=1}^{N_2} \beta_i(t)\psi_i(\theta), \tag{10}$$

where N_2 is the number of nodes at the back surface of the hemisphere, β_i are the unknown coefficients at those nodes, and $\{\psi_i(\theta)\}$ are the linear basis functions. The explicit Euler method was used as the predictor to provide a good initial guess to the implicit Euler method which was used as the corrector. Iterations were performed on the corrector until the error in the Euclidean norm fell below 10^{-7}. The matrix to be inverted at each iteration in the corrector step was a combination of a Jacobian matrix similar to that previously defined, a mass matrix, the elements of which were defined as

$$M_{ij} = \int_0^{\pi}\int_0^{R} \phi_i \phi_j r^2 \sin\theta \, d\theta \, dr,$$

and entries due to Eq. (6). See Poslinski and Tsamopoulos (*25*) for more details on the numerical procedure.

The only unknown parameters in the model are the two rate constants, k_1 and k_2. Specific values for these constants are not available; however, global kinetic data can be used to determine the values of these rate constants. The data reported by Wigmans and Moulijn (*7*) are particularly useful in this respect because they report both the global rate and the average size of the catalyst particles.

The value of the rate constant k_1 was determined using the steady-state model. The solubility and diffusivity of carbon at 990 K were used in the model with a nickel particle of radius R = 3 nm. The value of k_1 was varied until the calculated rate of gasification was equal to that reported. The nickel catalyst deactivates in the experimental runs, so the match was made using the initial

rate of reaction before the degree of deactivation had become significant. This procedure was repeated using a temperature of 775 K. The two values for k_1 which resulted were then used to calculate a frequency factor and an activation energy for the rate constant k_1. It is important to note that this rate constant is different than that found directly from the kinetic data because the latter includes the effects of diffusivity and solubility.

Once k_1 was determined, the unsteady model was used to estimate the value of k_2. The values of solubility, diffusivity, and k_1 for 975 K were used in the model, with a particle radius of $R = 3$ nm. The value of k_2 was varied until the time required for catalyst deactivation matched that which has been reported. This procedure was repeated at a second temperature, $T = 775$ K, to find a second value for k_2 allowing a frequency factor and an activation energy to be calculated.

RESULTS AND DISCUSSION

The values determined for the surface reaction rate constants were used to determine the activation energy and frequency factor according to the Arrhenius relation. Equation (11) presents the results for both reactions:

$$k_1' = 2.05 \times 10^{-3}\ \text{mol cm}^{-2}\,\text{s}^{-1} \exp\{(-48.8\ \text{kJ mol}^{-1})/RT\} \quad (11a)$$

$$k_2' = 1.08 \times 10^{16}\ \text{s}^{-1} \exp\{(-167\ \text{kJ mol}^{-1})/RT\}. \quad (11b)$$

In the case of k_1 there is little uncertainty because it is chosen such that a computed value of the rate and an experimental value for the rate match. For k_2 there is more uncertainty, because the value is chosen so as to give the best match to the reported deactivation profile, not to a single numerical value.

1. Steady-State Model

Figure 2 shows how the steady-state model predicts that the rate of reaction will depend upon the size of the catalyst particle at a number of different temperatures. For each temperature the rate is normalized to the rate predicted for a 20-nm particle. The figure also shows experimental data which were measured by Baker and Sherwood (*5*) using *in situ* transmission electron microscopy to follow the rate of different sized particles. While the experimental data are for gasification of graphite (i.e., they are for two-dimensional channeling, not three-dimensional tunneling) the general shape of such a curve for an active carbon would be expected to be the same. (The present authors are not aware of any controlled atmosphere electron microscopy data of this kind for an active carbon.) The model clearly displays the same type of behavior as the experimental data.

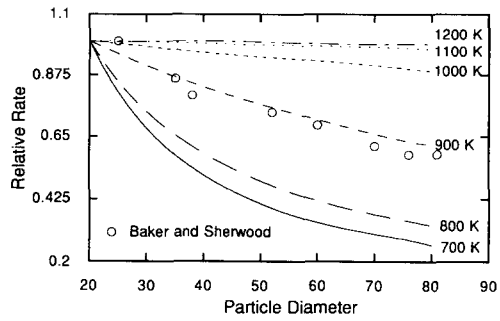

FIG. 2. A comparison of the computed dependence of the rate of reaction upon particle size at various temperatures to experimental data. Rates at each temperature are normalized by the rate of a 20-nm particle whereas experimental data are normalized by the rate of a 25-nm particle.

The present model can be used for much more than just explaining the observed rate versus particle diameter. Figure 2 shows that the rate versus diameter behavior changes as the reaction temperature changes. At lower temperatures the behavior is like that reported from experimental observation whereas at higher temperatures the dependence becomes much weaker. The experimental data shown in Fig. 2 were recorded at a temperature of 1423 K, yet they seem to correspond to behavior predicted

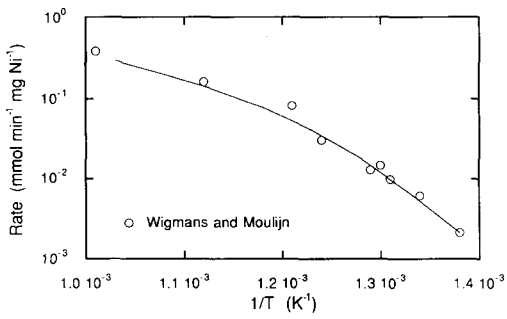

FIG. 3. A comparison of the computed Arrhenius plot using a particle radius of 0.3 nm to experimental data.

by the model at around 900 K. Both the experimental study and the modeling involved a nickel catalyst, however.

It appears that under the conditions of the experiment the catalyst particles were actually nickel oxide, and hence the diffusion coefficient would be expected to be lower than that of the metal. Indeed, the uncatalyzed reaction was observed to begin before the catalyzed reaction in the experimental study (*5*). A later experimental reexamination of the system has revealed catalytic activity at much lower temperatures than initially reported (*26*). Nonetheless, the model does predict the same shape for the rate versus particle diameter curve as has been observed experimentally. The change in the shape of the rate versus diameter plot with temperature is related to another experimental observation, namely a change in the apparent activation energy.

This is more easily seen in Fig. 3 which compares the prediction of the steady-state model to experimental data in an Arrhenius plot. The rate constant k_1 would of course be a straight line on this plot. To generate this figure, the model was used to calculate the global rate (which includes the effects of solubility and diffusivity) as a function of temperature. The particle size used was that reported by Wigmans and Moulijn (*7*), and for comparison their experimental data are also plotted. It is the two experimental data at 775 K and 990 K shown in the figure which were used to determine the value of k_1. The change in the experimental apparent activation energy has been observed in several studies of this reaction (*6, 7*). In most cases it has been assumed that at the higher temperatures the rate of external diffusion of the gaseous species to and from the catalyst has become rate limiting, even though in some studies experimental conditions were tested to ensure that diffusional limitations were not present.

From Fig. 2, an entirely different conclusion is drawn. At low temperatures the rate of diffusion of carbon through the metal is the rate-determining step. This results in a significant variation in the concentration of carbon across the rear surface of the catalyst particle, and this in turn manifests itself in the strong dependence of the rate of gasification upon particle size. In contrast, at high temperatures the diffusion of carbon through the metal is no longer rate determining. The concentration of carbon everywhere in the particle is nearly the same and equal to the solubility of carbon in nickel. This in turn results in a very weak dependence of the rate of reaction upon particle size.

This is further supported in that the apparent activation energy reported in experimental studies for the low-temperature gasification region is ca. 170 kJ mol^{-1}. The activation energy for the diffusion coefficient of carbon in nickel is 168 kJ mol^{-1}. This value is also significantly larger than the activation energy for surface reaction as determined from the model (see Eq. (11a)) or gas diffusion. Consequently, increases in temperature result in much larger increase in the rate of solid-state diffusion than in any other process. In fact, it is generally accepted that the rate-limiting step in the growth of carbon filaments (a reaction which is nearly the inverse of gasification) is the diffusion of carbon through the metal. The decrease in the rate at higher temperatures can be attributed to a change in the rate-

determining step from carbon diffusion through the particle to surface reaction on the particle.

The model is not detailed enough to pinpoint exactly the cause of the low apparent activation energy at high temperatures. There are five factors which affect the rate of the surface reaction: bulk diffusion within the metal, the solubility of carbon in the metal, the equilibration between the dissolved carbon just below the surface and the surface, the surface reaction rate constant, and the concentration of adsorbed oxygen on the surface. The model treats the first two of these explicitly, but it lumps all the latter three in the surface rate constant. As a result, the surface rate constant encompasses a true rate constant as well as equilibrium constants for oxygen adsorption and for the equilibration between subsurface carbon and surface carbon. This explains why the activation energy for the rate constant given in Eq. (11a) and used in the model is so low (48.8 kJ mol^{-1}).

Very careful studies of the temperature-programed oxidation of surface carbon on single crystal nickel surfaces (*27*) have indicated that the activation energy for the true surface rate constant is 134 kJ mol^{-1}, but these studies provide no value for the frequency factor. Similar single crystal studies indicate that an isotherm similar to the Langmuir adsorption isotherm is appropriate to describe the relationship between the concentration of carbon dissolved just below the surface and the fractional coverage of the surface by carbon (*28–30*). The constants in this equation are very dependent upon which crystal face of nickel is used. Hence, these studies are of limited utility in the present model, because it is not known which crystal faces are exposed by the small catalyst particles during gasification. Finally, the amount of oxygen adsorbed on the surface at high temperature and under reaction conditions has not been studied. Hence, to rigorously model each of these three effects would require the introduction of numerous unknown constants. In light of the excellent job the model does (Fig. 3) using the lumped rate constant and essentially no unknown constants (which effectively become adjustable parameters) such rigorous modeling was not deemed justified for the steady-state system.

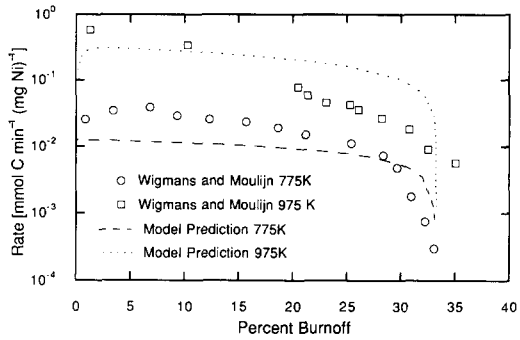

FIG. 4. A comparison of computed deactivation profiles to experimental data.

2. *Unsteady Model*

Figure 4 shows that the unsteady model is capable of a qualitative description of the deactivation process which accompanies catalytic gasification. The model was used to calculate the deactivation profile at several temperatures. Consistent with experimental observation (*3, 7, 11, 12*), it predicted that the amount of carbon which is gasified prior to the deactivation of the catalyst is essentially constant in the range from 35 to 40% irrespective of the temperature. Experimental data are again shown for comparison (*7*). Furthermore, the time scale for the particle to attain a pseudo-steady-state concentration profile was found to be very small compared to the time scale for catalyst deactivation in agreement with previous work (*8*). A closer examination of the model, however, reveals that it really is inadequate in several respects. These inadequacies are due to the lumping of three phenomena into one rate constant as described in the previous section.

First of all, it should not be necessary to

formulate two models; it should be possible to formulate a single model which has predictive ability with regard to the deactivation phenomenon. At present, prior knowledge is used to decide whether or not the catalyst will deactivate, and based upon this knowledge either the steady-state model or the unsteady model is used. There are two reasons underlying this. One reason is that the model does not include any input regarding the carbon which is being gasified.

In both forms of the model it is assumed that the leading point of the catalyst particle is saturated with carbon. Saturation is defined with respect to graphite which has a thermodynamic carbon activity equal to 1.0. Thus, by assuming that the leading point of the catalyst is saturated with carbon, it is assumed that the activity of the carbon dissolved in the metal at this point is equal to 1.0. When an activated carbon or coal char is used, its carbon activity is actually greater than 1.0 (i.e., there is a thermodynamic driving force for the conversion of these forms of carbon into graphite). This in turn means that the concentration of carbon dissolved in the metal can be greater than the classical solubility of carbon in the metal (*31*). This leads to the second reason why the model does not have the ability to predict deactivation as it is presently formulated.

Clearly, if the activity of carbon is just unity at the leading point, it will be less than unity everywhere else within the particle. (It is a gradient in the activity which leads to solid-state diffusion, not a gradient in the concentration (*32, 33*).) Thus, at the surface there will be no driving force for the formation of a deactivating graphitic overlayer. In the present model, the graphitic layer is allowed to form regardless of the carbon activity. Furthermore, the carbon surface coverage, Θ_C, varies with temperature in the same way that the carbon solubility does. The model can be given predictive ability with regard to deactivation if the following adjustments are made: (1) at the leading point the activity of the carbon in the metal should just equal the activity of the carbon substrate (i.e., an experimentally measured value greater than unity), (2) the diffusion equation should be recast in terms of activity gradients, not concentration gradients, (3) an isotherm relating the surface fractional coverage on the rear surface to the activity of carbon just below the surface must be developed (*28–30*) (recall that the present model simply sets the surface fractional coverage equal to the atomic fraction just below the surface), and (4) a rate expression for the reaction leading to the formation of a graphitic overlayer must be developed which will be equal to zero if the carbon activity is less than unity. If these modifications are made, the simple kinetic expression used for the deactivation reaction may not be adequate. In addition, an isotherm which provides the fractional surface coverage of oxygen as a function of temperature is needed as discussed in the previous section.

If all these modifications were incorporated into the model, there would be at least four unknown parameters: the rate constant for the deactivation reaction (frequency factor and activation energy) and the equilibrium constant for the oxygen coverage (Gibbs free energy change and enthalpy change). Further, the relationship between the activity of the carbon dissolved just below the surface and the fractional surface coverage involves another equilibrium constant and consequently two more parameters. These could either be assumed to equal those for one particular single crystal surface, or else they, too, would be unknown. The end result is a model with four to six parameters.

Experimental studies have shown that the amount of carbon which is gasified prior to the deactivation of the catalyst can be increased to greater than 50% if the gasification is conducted under a steadily increasing temperature program. The model was used to compute the deactivation profile under these circumstances, but it failed to reproduce the experimental findings. Instead, the results of the calculations showed virtually

no change in the amount of carbon gasified prior to catalyst deactivation for all practical temperature programing rates. At that point, the model was modified along the lines just discussed, but it was felt that the large number of unknown parameters made the problem little more than a curve fitting exercise.

CONCLUSIONS

The steady-state model based upon the solid-state diffusion of carbon through the catalyst particle does a good job of predicting both the particle size dependence of the gasification rate and the Arrhenius behavior. This is true even though the reaction rate constant lumps together three phenomena: the true rate constant, the equilibration of adsorbed oxygen with the gas phase, and the equilibration between the carbon dissolved just below the surface and the surface carbon. Decoupling these three phenomena would introduce more adjustable parameters into the model since data for all these phenomena are not available.

The steady-state model offers a new explanation for the experimentally observed change in the apparent activation energy at higher temperatures. In the past this had been attributed to the onset of external mass transfer limitations as often observed in heterogeneous catalysis. The model suggests that instead it may arise from a change in the rate-limiting process from one of solid-state diffusion of carbon through the catalyst particle to one of surface reaction. This is consistent with the apparent activation energy observed at the lower temperatures which is nearly indentical to the activation energy for the diffusion of carbon in nickel.

The modifications necessary for the extension of the model to the unsteady case have been identified. At present too many of the constants involved (each of which consists of a preexponential and an exponential term) are not available, giving the resulting model a plethora of adjustable parameters. Specific data are needed for the surface oxygen coverage as a function of temperature, the rate constant for the surface deactivation reaction, and the surface carbon coverage versus the subsurface carbon concentration as a function of temperature.

ACKNOWLEDGMENT

The support of this work by the NSF, Grant No. CBT-8857100, is gratefully acknowledged.

REFERENCES

1. McKee, D. W., *Carbon* **12,** 453 (1974).
2. Wigmans, T., van Doorn, J., and Moulijn, J. A., *Carbon* **19,** 309 (1981).
3. Colle, K. S., Kim, K., and Wold, A., *Fuel* **62,** 155 (1983).
4. Tamai, Y., Wantanabe, H., and Tomita, A., *Carbon* **15,** 103 (1981).
5. Baker, R. T. K., and Sherwood, R. D., *J. Catal.* **70,** 198 (1981).
6. Marsh, H., and Adair, R. R., *Carbon* **13,** 327 (1975).
7. Wigmans, T., and Moulijn, J. A., *in* "New Horizons in Catalysis" (T. Seiyama and K. Tanabe, Eds.), Stud. Surf. Sci. Catal., Vol. 7A, p. 501. Elsevier, New York, 1981.
8. Lund, C. R. F., *in* "Catalysis 1987" (J. W. Ward, Ed.) Stud. Surf. Sci. Catal., Vol. 38, p. 733. Elsevier, New York, 1988.
9. Carrazza, J., Chludzinski, J. J., Jr., Heinemann, H., Somorjai, G. A., and Baker, R. T. K., *in* "Ext. Abstr. Program-Bienn. Conf. Carbon 18th, 507, 1987,"
10. Carrazza, J., Tysoe, W. T., Heinemann, H., and Somorjai, G. A., *J. Catal.* **96,** 234 (1985).
11. Kim, K., Kershaw, R., Dwight, K, Wold, A., and Colle, K., *Mater. Res. Bull.* **17,** 591 (1982).
12. Lund, C. R. F., *J. Catal.* **95,** 71 (1985).
13. Choi, A. S., Devera, A. L., and Hawlay, M. C., *J. Catal.* **106,** 313 (1987).
14. Goethel, P.J., and Yang, R. T., *J. Catal.* **111,** 220 (1988).
15. Tsamopoulos, J. A., Dandekar, H. W., and Scholtz, J. H., *J. Catal.* **117,** 549 (1989).
16. Baker, R. T. K., Sherwood, R. D., and Dumesic, J. A., *J. Catal.* **62,** 221 (1980).
17. Goodman, D. W., Kelley, R. D., Madey, T. E., and Yates, J. T., Jr., *Prepr. Div. Pet. Chem. Amer. Chem. Soc.* **23,** 446 (1978).
18. Holstein, W. L., and Boudart, M., *Lat. Amer. J. Chem. Eng. Appl. Chem.* **13,** 107 (1983).

19. Tibbetts, G. G., Devour, M. G., and Rodda, E. J., *Carbon* **25,** 367 (1987).
20. Baker, R. T. K., *Catal. Rev. Sci. Eng.* **19,** 161 (1979).
21. Lander, J. J., Kern, H. E., and Beach, A. L., *J. Appl. Phys.* **23,** 1305 (1952).
22. Massaro, T. A., and Petersen, E. E., *J. Appl. Phys.* **42,** 5534 (1971).
23. Kovenskiy, I. I., *Fiz. Met. Metalloved.* **16,** 613 (1963).
24. Strang, G., and Fix, G. J., "An Analysis of the Finite Element Method." Prentice-Hall, NJ, Englewood Cliffs, 1973.
25. Poslinski, A. J., and Tsamopoulos, J. A., *Chem. Eng. Sci.*, in press.
26. Baker, R. T. K., Chludzinski, J. J., Jr., and Sherwood, R. D., *Carbon* **23,** 245 (1985).
27. Keleman, S. R., and Krenos, J., *Surf. Sci.* **157,** 491 (1985).
28. Shelton, J. C., Patil, H. R., and Blakeley, J. M., *Surf. Sci.* **43,** 493 (1974).
29. Eizenberg, M., and Blakeley, J. M., *J. Chem. Phys.* **71,** 3467 (1979).
30. Isett, L. C., and Blakeley, J. M., *Surf. Sci.* **58,** 397 (1976).
31. Wada, T., Wada, H., Elliott, J. F., and Chipman, J., *Metall. Trans.* **4,** 2199 (1971).
32. Darken, L. S., *Trans. AIME* **180,** 430 (1949).
33. Lund, C. R. F., and Yang, R. T., *Carbon* **27,** 956 (1989).